International Journal of Heat and Fluid Flow 30 (2009) 150–157

Contents lists available at ScienceDirect

International Journal of Heat and Fluid Flow

journal homepage: www.elsevier.com/locate/ijhff

Heat transfer by convection, conduction and radiation in solar chimney systems for ventilation of dwellings

H.F. Nouanégué, E. Bilgen *,[1]

Ecole Polytechnique, C.P. 6079 Centre Ville, Montreal Qc, Canada H3A 3A7

ARTICLE INFO

Article history:
Received 3 April 2008
Received in revised form 20 August 2008
Accepted 22 August 2008
Available online 28 November 2008

Keywords:
Solar chimney
Conjugate heat transfer
Natural convection
Radiation
Conduction
Numerical simulation

ABSTRACT

Numerical study by conjugate heat transfer is carried out of solar chimney systems for heating and ventilation of dwellings. Conservation equations are solved by finite difference-control volume numerical method. The governing parameters were: the Rayleigh numbers from 5×10^8 to 10^{11}, the Prandtl number, $Pr = 0.7$, constant for air, the chimney aspect ratio, $A = H/L$ from 6 to 15, the air channel width $l'/L = 0.2$ to 0.5, the air entrance port size, $h/L = 0.167$–0.667, the wall thickness $l/L = 0.25$–0.4, the conductivity ratio k_r from 5 to 50 and the surface emissivity, ε from 0 to 1. The Nusselt number, the dimensionless volume flow rate $\dot{V}$ and radiation heat flux ratio q_r/q_{tot} are calculated as a function of the governing parameters, and streamlines and isotherms are produced. The results show that the surface radiation modifies the flow and temperature fields, affects the Nusselt number and the volume flow rate, both in a positive way, and improves the ventilation performance of the chimneys.

1. Introduction

Chimneys or channels are used in various applications such as heating and ventilating of buildings, drying of agricultural products, and various other passive systems such as for cooling electronic components (e.g. Bar-Cohen and Krauss, 1988; Bilgen and Michel, 1979; Ekechukwa and Norton, 1999). The simplest chimney may be vertical channels without any thermal mass (Aung et al., 1972; Rheault and Bilgen, 1988). Solar chimneys are systems, which consist of a surface with glazing oriented towards sun, a massive wall which may be solid or liquid filled reservoir, an air channel in between and air ventilation ports (Ben Yedder and Bilgen, 1991). In many countries the glazing material is an expensive item and instead, an indigenous technique such as a wall of adobe brick facing the sun may be used as the surface to receive solar radiation (Bouchair, 1994). In any case, in all solar chimneys for heating and ventilation, heat transfer is usually conjugate, by convection, conduction and radiation, which must be studied simultaneously. Since early 1970s, the chimney systems combining a thermal mass have been studied experimentally (e.g. Bansal et al. (2005)), analytically (e.g. Ong and Chow (2003)) and numerically (e.g. Kim et al. (1990), Burch et al. (1985) and Bilgen and Yamane (2004)). Among the numerical studies, the conjugate heat transfer by convection and conduction has been considered in (Ben Yedder and Bilgen, 1991; Kim et al., 1990; Burch et al., 1985; Bilgen and Yamane, 2004), that by convection and radiation in (Moshfegh and Sandberg, 1996; Bouali and Mezrhab, 2006; Cadafalch et al., 2003) and by all three modes in (Lauriat and Desrayaud, 2006; Hall et al., 1999; Rao, 2007). We will briefly review those that are relevant to the present study.

Solar chimney may be described as a channel with two walls where an air movement is generated by buoyancy force generated by solar energy. The basic problem without considering conduction and surface radiation was studied in (Aung et al., 1972; Rheault and Bilgen, 1988). Both were on developing free convection in vertical channels, with asymmetric heating by Aung et al. (1972) and with non-isothermal vertical plates by Rheault and Bilgen (1988). In later numerical works, the conjugate heat transfer by free convection and conduction in vertical channels was studied by Kim et al. (1990), Burch et al. (1985) and Bilgen and Yamane (2004). Conjugate heat transfer by convection and conduction in systems having a glazing, solid wall and ventilation ports was numerically studied to determine their thermal performance in heating and ventilating of buildings by solar energy (e.g. Ben Yedder and Bilgen (1991) and references therein). Conjugate heat transfer by convection and surface radiation was studied numerically by Moshfegh and Sandberg (1996). They considered a vertical channel heated from one side with constant heat flux and insulated on the other side, and with various aspect ratios. They studied heat transfer by turbulent natural convection and surface radiation and revealed the importance of surface radiation on fluid flow in the channel. Bouali and Mezrhab (2006) studied heat transfer by laminar free convection and surface radiation in a divided vertical channel with

* Corresponding author. Tel.: +1 514 340 4711x4579; fax: +1 514 340 5917.
E-mail address: bilgen@polymtl.ca (E. Bilgen).
[1] Deceased author.

0142-727X/$ - see front matter © 2008 Published by Elsevier Inc.
doi:10.1016/j.ijheatfluidflow.2008.08.006

Nomenclature

A	aspect ratio, H/L
C_p	heat capacity, J/kg K
F_{ij}	Configuration factor
g	acceleration due to gravity, m/s^2
H	chimney height, m
h	air entrance port size, m
k	thermal conductivity, W/m K
k_r	solid to fluid thermal conductivity ratio, = k_s/k_f
L	chimney width, m
l	wall thickness, m
l'	channel width, m
N_r	radiation number, = $\frac{\sigma T_\infty^4}{q''}$
Nu	Nusselt Number
p	pressure, Pa
P	dimensionless pressure, = $(p-p_\infty)L^2/\rho\alpha^2$
Pr	Prandtl number, = ν/α
q''	heat flux, W/m^2
q	dimensionless heat flux, = $k_r\frac{\partial\theta}{\partial X}$
q_c	convective heat flux, W/m^2
q_r	radiative heat flux, W/m^2
q_t	total heat flux, W/m^2
Q	dimensionless volume flow rate through the channel
Ra	Rayleigh number, = $g\beta q'' L^4/(\nu\alpha k)$
T	temperature, K
U, V	dimensionless fluid velocities, = $uL/\alpha, vL/\alpha$
$\dot{V}$	dimensionless volume flow rate through the channel
X, Y	dimensionless Cartesian coordinates, = $x/L, y/L$

Greek symbols

α	thermal diffusivity, m^2/s
β	volumetric coefficient of thermal expansion, 1/K
Γ	general diffusion coefficient
δ_{ij}	Kronecker delta
ε	surface emissivity
ζ	dimensionless radiative heat flux, = $q_r/\sigma T_\infty^4$
υ	kinematic viscosity, m^2/s
ρ	fluid density, kg/m^3
Ψ	dimensionless stream function
θ	dimensionless temperature, = $(T-T_\infty)/(q''L/k_f)$
Θ	temperature ratio, = T/T_{infty}

Superscript

$\bar{}$	average

Subscripts

a	air
f	fluid
max	maximum
min	minimum
s	solid
∞	ambient value
$'$	at $X=1$, $Y=0$–A

isothermal sides and found that influence of surface radiation on the Nusselt number and mass flow rate was important at high Rayleigh numbers. Cadafalch et al. (2003) numerically studied heat transfer by natural convection and surface radiation in inclined channels isothermal on one side, insulated on the other, and derived a correlation for heat transfer as a function of relevant parameters. Conjugate heat transfer by convection, conduction and surface radiation in channels for different applications was studied in (Lauriat and Desrayaud, 2006; Hall et al., 1999; Rao, 2007). Lauriat and Desrayaud (2006) numerically studied heat transfer by the three modes in a channel with side ventilation ports and investigated interaction between surface radiation and convection. The active side walls were in contact with isothermal ambient air. They reported that the surface radiation decreased the hot active wall temperature but the change was negligible at the cold active wall. Hall et al. (1999) studied conjugate heat transfer by the three modes to investigate cooling of channel surfaces heated uniformly and symmetrically. They investigated optimum conditions for cooling and derived correlations useful for electronic cooling applications. In (Lauriat and Desrayaud, 2006; Hall et al., 1999), the radiosity – irradiation formulation was not used in the mathematical models. Rao (2007) studied conjugate heat transfer by free convection, conduction and surface radiation in vertical channels with insulated walls and discrete heat sources on one side. He determined the cooling performance in terms of relevant parameters.

In solar chimneys in particular, the heat transfer has been treated often analytically using empirical correlations; our literature study shows that in numerical studies, the conjugate nature of the problem is often neglected and solar chimney geometry is simplified to that of a vertical channel. Our aim in this paper is to carry out a numerical study on vertical solar chimneys with a practical geometry, which consist of two dimensional channel boarded by two solid walls. A constant heat flux is applied on one of the walls simulating the solar radiation and the other insulated, which may be the wall of a dwelling. Ambient air coming from the dwelling enters from a side port at the bottom and exits from the top. We will study conjugate heat transfer by convection, conduction and radiation and we will determine importance of each mode on the performance of the system as a function of governing geometrical and thermal properties.

2. Problem description and mathematical model

The system to study is shown in Fig. 1. It is a vertical channel bounded on the right and left by massive walls with a finite wall thickness and conductivity. A constant heat flux corresponding to solar radiation is imposed on the outer surface of the right wall. The left wall is insulated to simulate the conditions at the adjoining space. Air enters horizontally from the bottom on the left and discharged at the top. Boundary conditions are shown in Fig. 1.

2.1. Convection and conduction formulation

We assume that the fluid is Newtonian, and the third dimension has a negligible effect on the flow and heat transfer. With these assumptions, we use two dimensional conservation equations for mass, momentum and energy with Boussinesq approximation. By using L as the length scale, α/L as the velocity scale, Lq''/k_f as the temperature scale and $\rho\alpha^2/L^2$ for the pressure scale, we obtain following non-dimensional equations for convection and conduction.

$$\frac{\partial U}{\partial X}+\frac{\partial V}{\partial Y}=0 \tag{1}$$

$$U\frac{\partial U}{\partial X}+V\frac{\partial U}{\partial Y}=-\frac{\partial P}{\partial X}+\Gamma Pr\nabla^2 U \tag{2}$$

$$U\frac{\partial V}{\partial Y}+V\frac{\partial V}{\partial Y}=-\frac{\partial P}{\partial Y}+\Gamma Pr\nabla^2 V+RaPr\theta \tag{3}$$

$$U\frac{\partial \theta}{\partial X}+V\frac{\partial \theta}{\partial Y}=k_r\nabla^2\theta \tag{4}$$

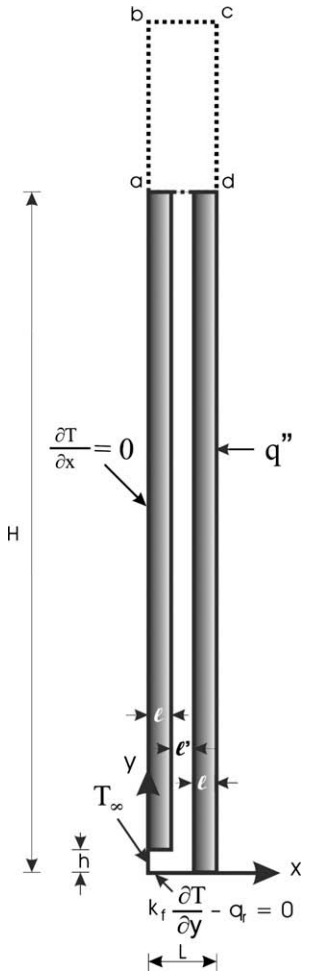

Fig. 1. Schematic of the system, the coordinates and the boundary conditions.

To ensure that $U = V = 0$ and the conduction is accounted for in the solid region, the value of Γ is specified as $\Gamma = 1$ in the fluid region and 10^{15} in the solid region. We have $k_r = 1$ in the fluid region and $k_r = k_s/k_f$ in the solid region in Eq. (4).

2.2. Radiation formulation

For the radiation formulation, an enclosure analysis is made using the evaluation of radiosity on the wall. The channel wall surfaces are assumed to be diffuse and grey. Openings are assumed to irradiate as a black body. The dimensional formulation of radiative heat exchange, we use the equation written in our notation given in (Siegel and Howell, 1981).

$$\sum_{j=1}^{N}(\delta_{ij}-F_{ij})\,\sigma T_j^4=\sum_{j=1}^{N}[\delta_{ij}-(1-\varepsilon_j)F_{ij}]\frac{q_{rj}}{\varepsilon_j} \tag{5}$$

For the non-dimensional formulation, a dimensionless temperature $\Theta = T/T_\infty$ is introduced and σT_∞^4 is used as a scale for radiation flux. The final non-dimensional energy conservation equation for a surface area is

$$\sum_{j=1}^{n}(\delta_{ij}-F_{ij})\,\Theta_j^4=\sum_{j=1}^{n}[\delta_{ij}-(1-\varepsilon_j)F_{ij}]\frac{\zeta_j}{\varepsilon_j} \tag{6}$$

where F_{ij} is the configuration factor and n is the total number of surface.

The energy balance on wall surfaces gives a relation between convective, conductive and radiative heat flux as

$$N_r\zeta=\left(\frac{\partial\theta_f}{\partial X}-k_r\frac{\partial\theta_s}{\partial X}\right) \tag{7}$$

where $N_r=\frac{\sigma T_\infty^4}{q''}$ is the radiation number, $\frac{\partial\theta_f}{\partial X}$ and $\frac{\partial\theta_s}{\partial X}$ are the heat fluxes from a wall surface to the fluid and that from the same surface to the solid wall, respectively.

The governing parameters are $Ra = g\beta q'' L^4/(\upsilon\alpha k)$, $Pr = \upsilon/\alpha$, k_r, ε, and $A = H/L$ and l/L.

The Nusselt number is calculated at the channel exit at $Y = A$ as

$$Nu=\frac{\int_0^1 V\theta|_{Y=A}\,dX}{\int_0^A \theta'\,dY} \tag{8}$$

The volume flow rate, Q is calculated as

$$Q=\int_{Y=A}V_{out}\,dX \tag{9}$$

where $V_{out} = V_{Y=A}$ if $V_{Y=A} > 0$ and $V_{out} = 0$ if $V_{Y=A} \leqslant 0$

The stream function is calculated from its definition as

$$U=-\frac{\partial\psi}{\partial Y},\quad V=\frac{\partial\psi}{\partial X} \tag{10}$$

ψ is zero on the solid surfaces and the streamlines are drawn by $\Delta\psi=(\psi_{max}-\psi_{min})/n$ with n as the number of increments.

2.3. Boundary conditions

They are for the computation domain including the extended domain shown in Fig. 1 with broken lines ab, bc and dc,

$$Y=0,\quad 0\leqslant X\leqslant 1-\ell/L: U=V=0,\quad \frac{\partial\theta}{\partial Y}-N_r\zeta=0 \tag{11}$$

$$Y=0,\quad 1-(\ell+\ell')/L\leqslant X\leqslant 1: U=V=0,\quad \frac{\partial\theta}{\partial Y}=0 \tag{12}$$

$$bc,\quad 0\leqslant X\leqslant 1:\frac{\partial V}{\partial Y}=-\frac{\partial U}{\partial X},\quad \frac{\partial U}{\partial Y}=0\quad \begin{cases}\frac{\partial\theta}{\partial Y}=0 \text{ if } V>0\\ \theta=0 \text{ if } V\leqslant 0\end{cases} \tag{13}$$

$$X=0,\quad 0\leqslant Y\leqslant h/L:\frac{\partial U}{\partial X}=-\frac{\partial V}{\partial Y},\quad \frac{\partial V}{\partial X}=0,\quad \theta=0 \tag{14}$$

$$X=0,\quad h/L\leqslant Y\leqslant H/L: U=V=0,\quad \frac{\partial\theta}{\partial X}=0 \tag{15}$$

$$X=0,\quad ab:\frac{\partial U}{\partial X}=-\frac{\partial V}{\partial Y},\quad \frac{\partial V}{\partial X}=0\quad \begin{cases}\theta=0 \text{ if } U>0\\ \frac{\partial\theta}{\partial X}=0 \text{ if } U\leqslant 0\end{cases} \tag{16}$$

$$X=1,\quad 0\leqslant Y\leqslant H/L: U=V=0,\quad k_r\frac{\partial\theta}{\partial X}=-1 \tag{17}$$

$$X=1,\quad cd:\frac{\partial U}{\partial X}=-\frac{\partial V}{\partial Y},\quad \frac{\partial V}{\partial X}=0\quad \begin{cases}\theta=0 \text{ if } U\leqslant 0\\ \frac{\partial\theta}{\partial X}=0 \text{ if } U>0\end{cases} \tag{18}$$

With the extended domain at the exit shown with abcd in Fig. 1, we carried out a study with six different boundary conditions at ab, bc and cd. The domain size was $0.3H$ by L with $A = 10$. We found that the relative variation of the Nusselt number among the six boundary conditions was 3.18% maximum and that of the volume flow rate through the channel was nil. On the other hand, the relative difference for the latter was 1.49% between the cases with and without extended domain, but no difference was found for the Nusselt number. Additionally, the deviations in both the Nusselt number and the volume flow rate with and without extended domain cases were higher for small values of ε and for higher values of the Rayleigh number. Thus, although the deviations were in the acceptable range with and without extended domain, we opted

for the extended domain and physically the most natural flow and temperature fields among the six boundary conditions. They are shown by Eqs. (13), (16), and (18); they satisfy the conservation of mass, no fluid acceleration through the boundary and allow backflow. We carried out also a similar study at the entrance with $3L$ by H extended domain on the left of the system and found similar results. We note that with the extended domain, the flow field was modified considerably at the entrance with more uniform velocity profile and an increased Nusselt number by 3.05% maximum at $Ra = 10^{11}$. The flow field in the channel and at the exit was however less influenced with very similar velocity profiles along the channel and at the exit. In this case, we opted for the case without extended domain because the computational domain became too large without advantage. Hence, we used the boundary condition given by Eq. (14).

3. Numerical procedure

The governing conservation equations of mass, momentum and energy, Eqs. (1)–(7) were solved simultaneously. Numerical solution of the governing equations for conduction and convection were obtained using a finite-volume employing the Alternating Direction Implicit (ADI) control volume with under-relaxation factor for temperature, velocities and pressure (Patankar, 1980). The radiation calculations were carried out using wall surface temperature to determine radiative heat flux by solving the linear equation system with the Gauss–Seidel method. Then the radiative heat flux on the radiative surfaces is introduced as a heat source in the calculation of temperature velocity and pressure field with SIMPLER algorithm. To ensure a better convergence, non-uniform grid in X and Y directions was used in the fluid domain, in all computations.

The grid independence study was carried out with the grid size from 15×90 to 45×260. We found that a 30×160 grid size was satisfactory with less than 3% deviation from that with grid size of 45×260 as presented in Table 1.

To verify the numerical method carefully and rigorously, the code was validated with the benchmark problem. Table 2 shows a comparison of the results with the benchmark (De Vahl Davis and Jones, 1983) and a benchmark quality study (Dixit and Babu, 2006). We see a maximum deviation of 1.96% from the benchmark and 1.95% from that of benchmark quality study. The code was also validated with the experimental work by Krishnan et al. (2004). The comparison is presented in Table 3, which is also satisfactory.

Table 3
Validation study with an open cavity (Krishnan et al., 2004)

	This study	Krishnan et al. (2004)
l' in mm	q_r/q_t	q_r/q_t
12.6	0.283	0.309
17.5	0.333	0.347
25.5	0.392	0.392
37.0	0.439	0.436
46.0	0.464	0.474
52.2	0.477	0.481

S is the heater size.

4. Results and discussion

The variable geometrical parameters considered are, the aspect ratio, $A = 6$, 10 and 15, and the dimensionless wall thickness, $l/L = 0.25$, 0.333 and 0.4 or the channel width, $l'/L = 0.20$, 0.333 and 0.5, the air entrance port size, $h/L = 0.167$, 0.333, 0.667. The Rayleigh number was varied from $Ra = 5 \times 10^8$ to 10^{11}. We note that following the definition of the Rayleigh number, $Ra = g\beta q'' L^4/(\upsilon\alpha k)$ for a given geometry and fluid, $Ra \sim q'' = q_t$. Thus Ra is varied by varying q_t. The surface temperature at a given height Y is directly proportional to the heat flux. Although the heat flux, q_t is constant along the wall, the inside surface temperatures increase in the flow direction due to convection along the channel.

We note also that the range of Ra covers the practical applications and the relatively high range is due to the scales used in the definition of Ra, which is used throughout as a common governing parameter. In reality, the corresponding Ra for convection should be smaller if we used the convective heat flux in the definition of Ra. In comparison with a vertical plate heated by constant heat flux, the transition to turbulent regime starts at $Ra > 2 \times 10^{13}$ (Chen et al., 2003).

The variable thermal properties were: the conductivity ratio, $k_r = 5$, 20, 50 and the surface emissivity, $\varepsilon = 0$ (corresponding to no radiation heat exchange), 0.1, 0.4, 0.7 and 1.0. The Prandtl number, $Pr = 0.70$ for air was kept constant. A typical solar chimney dimensions are $L = 0.3$ m, $H = 3$ m, the channel width and each wall thickness $l' = l = 0.10$ m, the entrance size $h = 0.10$ m. The conductivity ratio k_r varies from 5 to 50 for common materials such as plywood, adobe brick, concrete block, common brick, which may be used in solar chimneys. We will present first the results for the typical case with dimensionless parameters: $A = 10$, $l/L = 0.333$, $h/L = 0.333$, $k_r = 20$ and $\varepsilon = 0$, 0.4, 1.0; and then we will examine

Table 1
Grid convergence study

	Nu	%	Q	%	Ψ_{max}	%	θ_{max}	%	q_r/q_t	%
15×90	25.64	−16.35	2042.71	−8.66	2773.17	2.48	0.04	16.56	0.18	−35.89
24×130	29.94	−2.32	2386.54	6.71	2742.48	1.35	0.03	3.90	0.22	−20.04
30×160	30.55	−0.35	2176.48	−2.68	2726.77	0.77	0.03	2.98	0.27	−2.89
36×200	30.64	−0.04	2249.21	0.57	2744.03	1.40	0.03	2.15	0.28	−0.21
45×260	30.65	0.00	2236.40	0.00	2706.03	0.00	0.03	0.00	0.28	0.00

Table 2
Validation study with the benchmarks

Ra	This study	Nu		This study	U_{max}		This study	V_{max}	
		[1]	[2]		[1]	[2]		[1]	[2]
10^3	1.128	1.116	1.210	3.634	3.649	3.653	3.668	3.697	3.682
10^4	2.286	2.242	2.286	16.182	16.178	16.178	19.541	19.617	19.569
10^5	4.592	4.531	4.563	35.070	34.730	35.521	68.118	68.590	68.655
10^6	8.970	9.035	8.800	65.330	64.630	64.186	222.859	219.360	219.866

[1] – de Vahl Davis and Jones (1983) and [2] – Dixit and Babu (2006).

the effect of these parameters on the results. We will be using the Rayleigh number, $Ra = g\beta q'' L^4/k\alpha\nu$ to present both Nu, Q and q_r/q_t defined in the nomenclature. For the simulation of the system shown in Fig. 1, we specified $L = 0.3$ m, $T_\infty = 300$ K. We had the following range for the radiation number: $44.306 < N_r < 0.133$ at Ra from 5×10^8 to 10^{11}, respectively; i.e. N_r is a decreasing function of Ra.

We present Nu, q_r/q_t and Q as a function of Ra and ε as a parameter for the typical case in Fig. 2. Nu in Fig. 2a is an increasing function of Ra and ε. The first one is expected. We note that for the typical case of Fig. 2, the variation of Nu is weakly non-linear, following $Nu \sim Ra^{0.14}$, which is consistent with the literature (e.g. Onur et al. (1997)). Indeed, depending on the geometry and thermal conditions, they have found experimentally in vertical channels that $Nu \sim Ra^{0.12-0.35}$. The second, i.e. increasing relation of Nu with ε is due to the fact that the Nusselt number is proportional to the average air temperature times the average air velocity in the channel. The average air temperature decreases weakly with increasing emissivity while the average velocity increases strongly with it. As a result, Nu increases with ε. Indeed, at $Ra = 10^{11}$ for example, the average air temperature varies from 0.033 to 0.025 while the average air velocity or volume flow rate varies from 523 to 2176 for ε from 0 to 1. The variation in the first is about 22.4% and in the second 3.16 times. Thus, the Nusselt number increases considerably. We see in Fig. 2b that the non-dimensional radiative heat flux is insensitive to the variation of the Rayleigh number. This is because the average radiative heat flux q_r and the total heat flux q_t increases with the Rayleigh number almost at the same rate since in both cases the heat flux changes with the fourth power of the surface temperature. Indeed, for $k_r = 20$ for example, at $Ra = 10^9$, 10^{10} and 10^{11}, the average temperature difference between the left and right inside wall surfaces is $\Delta T = 2.59$, 19.88 and 66.01 K, respectively. At the corresponding Rayleigh numbers, the average radiative heat flux on the right wall is $q_r = 13.84$, 126.87 and 1401.56 W/m^2, and the total heat flux q_t is 34.95, 349.52 and 3495.15 W/m^2, respectively. The resulting q_r/q_t is 0.43, 0.36 and 0.40, which is almost the same. Nevertheless, we notice that q_r/q_t goes through a broad minimum at Ra from 10^9 to 10^{10}. Since $Ra \sim q_t \sim \Delta T$ the average inside wall temperature increases with Ra. On the other hand, the heat flux by surface radiation increases as $q_r \sim T^4$. We see from the values given above at $Ra = 10^9$, 10^{10} and 10^{11} that the total heat flux increases by an order of magnitude for Ra from 10^9 to 10^{10} and then 10^{11}, but q_r increases by 9.17 times from 10^9 to10^{10} and 11.05 times from 10^{10} and 10^{11}. Thus, although the variation of the total heat flux is linear with Ra, the variation of the surface radiation heat flux is non-linear, which results in the observed minimum. Following Nu versus Ra relation, the volume flow rate presented in Fig. 2c is also an increasing function of both Ra and ε. Nu is increased by 32% and 22% at $Ra = 5 \times 10^8$ and 10^{11}, respectively when ε is changed from zero to 1. Q is increased by 2 and 3.7 times at the same condition. We can see in Fig. 2 that the effect of surface radiation on Nu and Q is not negligible.

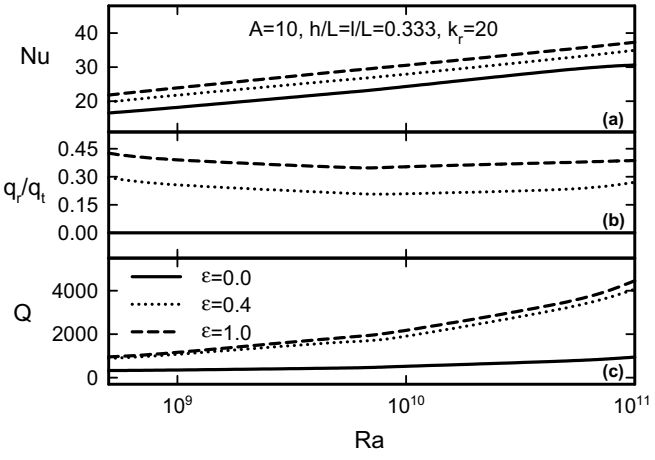

Fig. 2. Nu, q_r/q_t and Q as a function of Ra with $\varepsilon = 0.0$, 0.4 and 1.0 for the typical case of $A = 10$, $l/L = 0.333$, $h/L = 0.333$, $k_r = 20$.

To see the trends we discussed with Fig. 2, we produced streamlines (on the upper figures) and isotherms (on the lower figures) in the chimney for the typical case at $Ra = 10^9$, 10^{10} and 10^{11} for $\varepsilon = 0$ (shown on the left) and 1 (on the right) for each Ra number in Fig. 3a–c, respectively. To make a fair comparison, we used the same increments for $\Delta\Psi = 200$ and $\Delta\theta = 4 \times 10^{-3}$ throughout. In the upper figures for $\varepsilon = 1$, we see that the air makes a sharp turn at the lower part at the entrance section and flows in the vertical channel with higher gradients near the right wall and exits without any reverse flow. As Ra is increased, the gradients near the right wall are also increased. Indeed, $\Psi_{ext} = 1346$ ($X = 0.4151$, $Y = 0.6946$) at $Ra = 10^9$, $\Psi_{ext} = 2497$ ($X = 0.4151$, $Y = 0.6404$) at $Ra = 10^{10}$ and $\Psi_{ext} = 5029$ ($X = 0.4151$, $Y = 0.8128$) at $Ra = 10^{11}$. Similarly for the isotherms shown in the lower part of the figure, we see that as the Rayleigh number is increased the heat transfer becomes more intensive and the isotherms become parallel in the right vertical wall. The isotherms on the left wall show that temperature gradients in the vertical direction are higher at $Ra = 10^9$ and slightly lower at $Ra = 10^{10}$ and still lower at $Ra = 10^{11}$. That is, the left wall becomes temperature wise more uniform as the Rayleigh is increased. This is due to increased radiation heat exchange between the two wall surfaces. $\theta_{max} = 0.041$ ($X = 1.0$, $Y = 8.08$) at $Ra = 10^9$, $\theta_{max} = 0.033$ ($X = 1.0$, $Y = 8.35$) at $Ra = 10^{10}$ and $\theta_{max} = 0.026$ ($X = 1.0$, $Y = 8.08$) at $Ra = 10^{11}$. In contrast for $\varepsilon = 0$ at the left sides for each case, we observe a reverse flow at the exit, the gradients are higher at higher elevation of the channel and there is no temperature gradient at the left wall. The last one is expected since the heat transfer to the left wall is weak without radiative heat exchange. Correspondingly, Ψ_{ext} is lower by 57–70% and θ_{max} is higher by 24–18% at Ra from 10^9 to 10^{11}, respectively.

Similarly, we present in Fig. 4 Nu, q_r/q_t and Q as a function of Ra and k_r as a variable parameter for $\varepsilon = 0$ and 1. We observe again the same trend: Nu in Fig. 4a is increasing functions of Ra as well as k_r. For $\varepsilon = 0$ and 1 Nu is an increasing function of Ra, which is expected. It is also an increasing function of the surface emissivity ε as we have explained with Fig. 2. The Nusselt number Nu is an increasing function of k_r because the surface temperature $\theta_{X=1}$ in the denominator of Eq. (8) decreases with increasing conductivity ratio while the average temperature at inner surfaces of the channel as well as the volume flow rate is insensitive to k_r. For example, for $Ra = 10^{10}$, $\theta_{X=1}$ is equal to 0.784, 0.302 and 0.203 for $k_r = 5$, 20 and 50, respectively while θV across the channel is quasi-constant at about 9.02. As a consequence, Nu increases with k_r. We see in Fig. 4b and c that the radiative heat flux q_r/q_t and the volume flow rate Q are insensitive to the variation of k_r. This is because the surface temperature does not change appreciably with k_r. Indeed, for $Ra = 10^{10}$ for example, for $k_r = 5$, 20 and 50, the temperature difference between the right and left walls inside surfaces ΔT was 21.57, 19.88 and 19.69 K. Thus, q_r/q_t is 0.354, 0.363 and 0.340, respectively for $k_r = 5$, 20 and 50. As a result the effect of k_r on q_r/q_t is negligible and its magnitude is almost the same with about 40% of the total heat flux as in Fig. 2. In addition, q_r/q_t is an increasing function of the surface emissivity ε, the reason for which is explained also with Fig. 2. For $\varepsilon = 0$, i.e. without radiative heat exchange, the convection is relatively weak as a result of which the volume flow rate is similarly small. Otherwise for $\varepsilon = 1$, the volume flow rate Q has the same order of magnitude as in Fig. 2. We see from the results

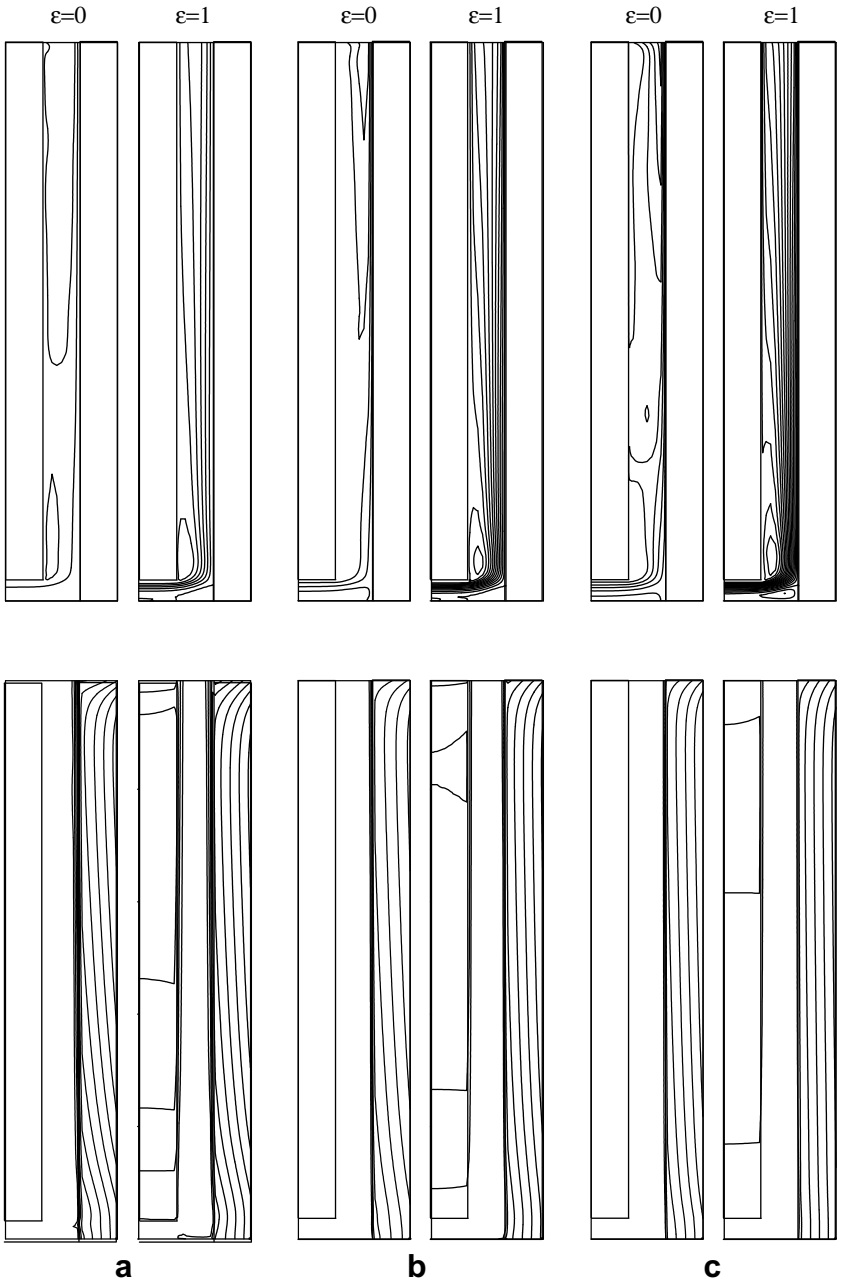

Fig. 3. Streamlines (in the upper part) and isotherms (in the lower part) for the typical case of $A = 10$, $l/L = h/L = 0.333$ and $k_r = 20$. In each pair of figures, the left one is with $\varepsilon = 0.0$ and the right one $\varepsilon = 1.0$. (a) $Ra = 10^9$, $\Psi_{ext} = 1346$ ($X = 0.4151$, $Y = 0.6946$) and $\theta_{max} = 0.041$ ($X = 1.0$, $Y = 8.08$), (b) $Ra = 10^{10}$, $\Psi_{ext} = 2497$ ($X = 0.4151$, $Y = 0.6404$) and $\theta_{max} = 0.033$ ($X = 1.0$, $Y = 8.35$) and (c) $Ra = 10^{11}$, $\Psi_{ext} = 5029$ ($X = 0.4151$, $Y = 0.8128$) and θ_{max}=0.026 ($X = 1.0$, $Y = 8.08$). Note: the extended computation domain is removed and only the chimney is shown.

with $\varepsilon = 0$ and 1 that the heat transfer is increased with surface radiation; for example, for $k_r = 50$, Nu is higher by about 30% when $\varepsilon = 1$.

We present a cross plot of Nu, q_r/q_t and Q as a function of ε at three Ra numbers in Fig. 5. We see that the effect of ε is immediate on q_r/q_t and Q: even at very low values of ε, the radiative heat exchange becomes considerable. It reaches a plateau after about $\varepsilon > 0.7$ for the radiative heat exchange in Fig. 5b and after about $\varepsilon > 0.5$ for the volume flow rate in Fig. 5c. The effect of ε on the convection is to increase it gradually as shown in Fig. 5a. At $Ra = 10^{11}$ for example, the increase in Nusselt number is about 30% and that in the volume flow rate is 3.7 times when the emissivity varies from zero to 1.

We show in Fig. 6 the effect of k_r on Nu, q_r/q_t and Q for the typical case at $Ra = 10^{10}$ and ε variable from 0 to 1. It is clear that as we discussed earlier with Fig. 4b and c q_r/q_t and Q is almost independent of k_r; in contrast, its effect is important on the convection heat transfer; for example, the Nusselt number is increased by 2.75 times when k_r is increased from 5 to 50.

The effect of the geometrical parameters, A, l/L and h/L on Nu, q_r/q_t and Q are shown in Figs. 7–9, respectively. They are for the typical case at $Ra = 10^{10}$ with ε as variable from 0 to 1.

We see in Fig. 7a that the effect of the aspect ratio, A on Nu is negligible when the surface radiation is considered. A slight decrease of Nu with the aspect ratio is due to increased flow rate through the chimney. On the other hand, in Fig. 7b q_r/q_t is a

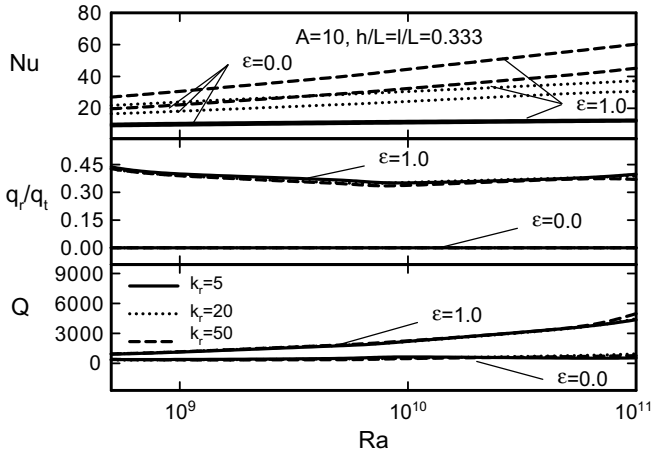

Fig. 4. *Nu*, q_r/q_{tot} and *Q* as a function of *Ra* with $\varepsilon = 0.0$ and 1.0 and $k_r = 5$, 20 and 50 for the typical case of $A = 10$, $l/L = 0.333$, $h/L = 0.333$.

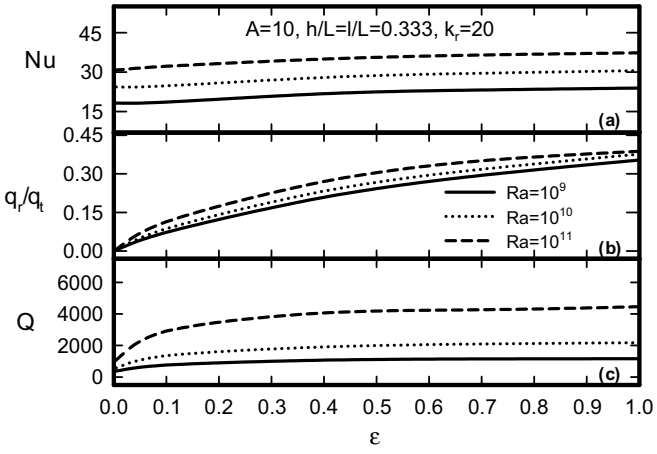

Fig. 5. *Nu*, q_r/q_t and *Q* as a function of ε with $Ra = 10^9$, 10^{10} and 10^{11} for the typical case of $A = 10$, $l/L = 0.333$, $h/L = 0.333$, $k_r = 20$.

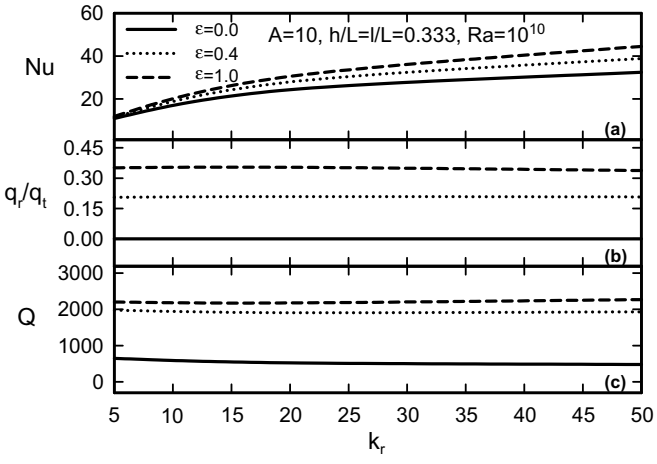

Fig. 6. *Nu*, q_r/q_t and *Q* as a function of k_r with $\varepsilon = 0.0$, 0.4 and 1.0 for the typical case of $A = 10$, $l/L = 0.333$, $h/L = 0.333$, $Ra = 10^{10}$.

decreasing function of *A*, in consequence of which the convective heat flux is increasing with increasing aspect ratio. Indeed, we found that the temperature difference between left and right walls is a decreasing function of the aspect ratio, although the surface

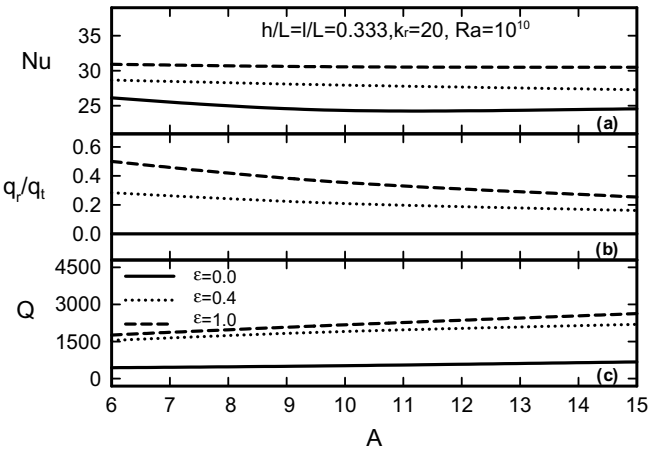

Fig. 7. *Nu*, q_r/q_t and *Q* as a function of *A* with $\varepsilon = 0.0$, 0.4 and 1.0 for the typical case of $l/L = 0.333$, $h/L = 0.333$, $k_r = 20$, $Ra = 10^{10}$.

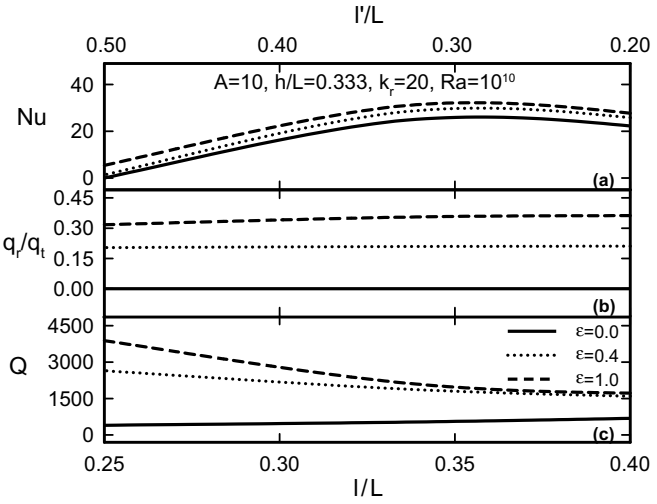

Fig. 8. *Nu*, q_r/q_t and *Q* as a function of l/L (the lower scale) and of l'/L (the upper scale) with $\varepsilon = 0.0$, 0.4 and 1.0 for the typical case of $A = 10$, $h/L = 0.333$, $k_r = 20$, $Ra = 10^{10}$.

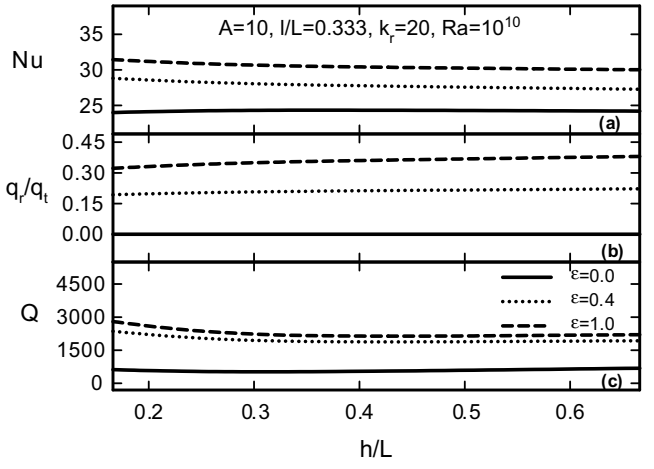

Fig. 9. *Nu*, q_r/q_t and *Q* as a function of h/L with $\varepsilon = 0.0$, 0.4 and 1.0 for the typical case of $A = 10$, $l/L = 0.333$, $k_r = 20$, $Ra = 10^{10}$.

temperature as well as the air temperature is increased as the aspect ratio is increased. Thus, we expect that the radiative heat flux be a decreasing function of A while the convective heat flux and air flow rate be an increasing function of it. In fact, we can observe in Fig. 7c that the volume flow rate is an increasing function of A; by increasing A from 6 to 15, the volume flow rate is increased by 50%.

We observe in Fig. 8 that at smaller wall thickness, i.e. larger channel width, l'/L shown in the upper scale in the figure, the convection is favored, hence the volume flow rate is increased; as a result, the Nusselt number is decreased. As the wall thickness is increased the volume flow rate decreases and Nu is increased. It appears that there may be an optimum wall thickness or optimum channel width to maximize the heat transfer by convection; for the typical case it is at about $l/L = 0.35$ or $l'/L = 0.30$. On the other hand, the volume flow rate is a decreasing function of the wall thickness although the effect of l/L becomes less important for $l/L > 0.35$ or $l'/L < 0.30$. The effect of l/L is negligible on q_r/q_t, which is an expected result.

The effect of h/L on Nu, q_r/q_t and Q shown in Fig. 9 is less significant. Nu in Fig. 9a is a slightly decreasing function of h/L for $\varepsilon > 0$ and almost constant for $\varepsilon = 0$. The effect of h/L in Fig. 9b is negligible on q_r/q_t, which is expected. We see in Fig. 9c that ssimilar to the effect of l/L, we have an improvement of about 25–30% in the volume flow rate when h/L is small and $\varepsilon > 0$. For $\varepsilon = 0$, the volume flow rate is an increasing function of h/L; the improvement is about 10% when h/L is increased from 0.25 to 0.4.

5. Conclusion

We studied conjugate heat transfer by natural convection, conduction and radiation in vertical solar chimneys boarded by two solid walls with finite conductivity. The constant heat flux is imposed on one of the active walls, the other being insulated. We developed a mathematical model, a numerical code and solved simultaneously coupled conservation equations of mass, momentum and energy by finite difference method using SIMPLER algorithm. In view of the results presented, the findings in this study may be helpful for designers of solar chimneys.

The radiative heat flux ratio, q_r/q_t increases rapidly at low surface emissivity and reaches about 0.4 at $\varepsilon = 1$. The radiative heat flux is a strong increasing function of the surface emissivity starting at its low values and reaching a plateau for $\varepsilon > 0.7$. Considering that the surface emissivity for many practical materials is in the range of 0.7–0.9, it is clear that the radiative heat transfer is not negligible in solar chimney systems.

The surface radiation modifies the flow and temperature fields. In particular, the flow on the active wall is modified; the velocity gradient is increased. While the surface radiative heat exchange does not change much, the volume flow rate as well as heat transfer by natural convection are increased with the Rayleigh number. The role of surface temperature for the q_r/q_t ratio is not negligible; at low Rayleigh numbers it may be up 42%.

The Nusselt number by natural convection is an increasing function of the surface emissivity, the conductivity ratio and the wall thickness. It is insensitive to variation of the aspect ratio and the entrance port size.

The volume flow rate is an increasing function of the Rayleigh number, the surface emissivity and the chimney aspect ratio. It is a decreasing function of the wall thickness and the entrance port size. It is insensitive to variation of the conductivity ratio.

Acknowledgement

The financial support for this study by Natural Sciences and Engineering Research Council Canada is acknowledged.

References

Aung, W., Fletcher, L.S., Sernas, V., 1972. Developing laminar free convection between vertical flat plates with asymmetric heating. Int. J. Heat Mass Transfer 15, 2293–2304.
Bansal, N.K., Mathur, J., Mathur, S., Jain, M., 2005. Modeling of window-sized solar chimneys for ventilation. Build. Environ. 40, 1302–1308.
Bar-Cohen, A., Krauss, A.D., 1988. Advances in Thermal Modeling of Electronic Components and Systems. Hemisphere Publishing Corporation, New York.
Ben Yedder, R., Bilgen, E., 1991. Natural convection and conduction in Trombe wall systems. Int. J. Heat Mass Transfer 34, 1237–1248.
Bilgen, E., Michel, J., 1979. Integration of solar systems in architectural and urban design. In: Sayigh, A.A.M. (Ed.), Solar Energy Appl Build. Academic Press, New York.
Bilgen, E., Yamane, T., 2004. Conjugate heat transfer in enclosures with openings for ventilation. Heat Mass Transfer 40, 401–411.
Bouali, H., Mezrhab, A., 2006. Combined radiative and convective heat transfer in a divided channel. Int. J. Numer. Meth. Heat Fluid Flow 16, 84–106.
Bouchair, A., 1994. Solar chimney for promoting cooling ventilation in southern Algeria. Build. Service Eng. Res. Technol. 15, 81–93.
Burch, T., Rhodes, T., Acharya, S., 1985. Laminar natural convention between finitely conducting vertical plates. Int. J. Heat Mass Transfer 28, 1173–1186.
Cadafalch, J., Oliva, A., van der Graaf, G., Albets, X., 2003. Natural convection in a large, inclined channel with asymmetric heating and surface radiation. J. Heat Transfer 125, 812–820.
Chen, Z.D., Bandopadhayay, P., Halldorsson, J., Byrjalsen, C., Heiselberg, P., Li, Y., 2003. An experimental investigation of a solar chimney model with uniform wall heat flux. Build. Environ. 38, 893–906.
De Vahl Davis, G., Jones, I.P., 1983. Natural convection in square cavity: a comparison exercise 3, 227–248.
Dixit, H.N., Babu, V., 2006. Simulation of high Rayleigh number natural convection in a square cavity using the lattice Boltzmann method. Int. J. Heat Mass Transfer 49, 727–739.
Ekechukwa, O.V., Norton, B., 1999. Review of solar energy drying system II. An overview of solar drying technology. Energy Conserv. Manage. 40, 615–655.
Hall, D., Vliet, G.C., Bergman, T.L., 1999. Natural convection cooling of vertical rectangular channels in air considering radiation and wall conduction. J. Electron. Pack. 121, 75–84.
Kim, S.H., Anand, N.K., Aung, W., 1990. Effect of wall conduction on free convection between asymmetrically heated vertical plates. Uniform wall heat flux. Int. J. Heat Mass Transfer 33, 1013–1023.
Krishnan, A.S., Premachandran, B., Balaji, C., Venkateshan, S.P., 2004. Combined experimental and numerical approaches to multi-mode heat transfer between vertical parallel plates. Experiment Therm. Fluid Sci. 29, 75–86.
Lauriat, G., Desrayaud, G., 2006. Effect of surface radiation on conjugate natural convection in partially open enclosures. Int. J. Therm. Sci. 45, 335–346.
Moshfegh, B., Sandberg, M., 1996. Investigation of fluid flow and heat transfer in a vertical channel heated from one side by PV elements. Part I – numerical study. In: Proceeding of the 1996 World Renewable Energy Congress on Renewable Energy, Energy Efficiency and the Environment. Part 1, June 15–21, 1996. Renewable Energy, Pergamon Press Inc, Denver, CO, 248–253.
Ong, K.S., Chow, C.C., 2003. Performance of a solar chimney. Solar Energy 74, 1–17.
Onur, N., Sivrioglu, M., Aktas, M.K., 1997. Experimental study on the natural convection heat transfer between inclined plates. Heat Mass Transfer 32, 471–476.
Patankar, S.V., 1980. Numerical Heat Transfer and Fluid Flow. Hemisphere Publishing Corporation, New York.
Rao, C.G., 2007. Interaction of surface radiation with conduction and convection from a vertical channel with multiple discrete heat sources in the left wall. Numer. Heat Transfer Part A: Appl. 52, 831–848.
Rheault, S., Bilgen, E., 1988. Developing laminar convection between non-isothermal vertical plates. Proceeding of Collected Papers in Heat Transfer: Winter Annual Meeting of the American Society of Mechanical Engineers. ASME, Chicago, IL. 103–108.
Siegel, R., Howell, J.R., 1981. Thermal Radiation Heat Transfer, second ed. Hemisphere Publishing Corporation, Washington.